AC electrowetting promoted droplet shedding on hydrophobic surfaces

Cite as: Appl. Phys. Lett. **116**, 193701 (2020); doi: 10.1063/5.0006117
Submitted: 27 February 2020 · Accepted: 29 April 2020 ·
Published Online: 11 May 2020

Enakshi D. Wikramanayake, Jordin Perry, and Vaibhav Bahadur[a)]

AFFILIATIONS

Walker Department of Mechanical Engineering, The University of Texas at Austin, Austin, Texas 78712, USA

[a)]Author to whom correspondence should be addressed: vb@austin.utexas.edu

ABSTRACT

Condensation is significantly enhanced by condensing vapor as droplets (instead of a film), which rapidly shed-off. Electrowetting (EW)-induced coalescence and shedding of droplets have been recently shown to accelerate condensation. This work studies the influence of AC electrowetting fields on short-duration droplet shedding on hydrophobic surfaces. Experiments involve tracking the shedding of an ensemble of water droplets under the influence of EW fields, with three parameters being varied (voltage, AC frequency, and device geometry). Significant physical insights into EW-induced droplet shedding are obtained. First, EW enables almost complete removal of water (dry area fraction ~98%) in very short time durations (~ 1 s). Second, while the dry area fraction does depend on the applied voltage, significant water shedding can be achieved without needing to apply voltages significantly higher than the threshold voltage. Third, the frequency of the AC waveform does not influence the dry area fraction (for voltages above the threshold voltage); however the time constant associated with droplet shedding strongly depends on the AC frequency. Fourth, the orientation of the device influences water removal due to electrostatic pinning of droplets. Importantly, the measured water removal fluxes immediately after the application of an EW field are two orders of magnitude higher than those measured over a long-duration condensation experiment; this highlights the benefits of intermittent EW fields as opposed to continuous EW fields. Overall, these results suggest that EW on hydrophobic surfaces offers benefits comparable to those offered by superhydrophobic surfaces.

Condensation of water impacts processes involved in power generation,[1] desalination,[2,3] and water harvesting.[4–6] On metal surfaces (hydrophilic), vapor condenses as a film; the thermal resistance of this film substantially reduces heat transfer.[7] Condensing vapor as droplets, which then shed-off, eliminates the film resistance and enhances heat transfer by 5 to 10 times.[1,7,8] Many studies detail enhancement of dropwise condensation by modifying the chemistry/texture of the condensing surface[9–12] to promote condensate removal. Alternatively, there exist eight recent studies on electrowetting (EW)-enhanced dropwise condensation,[13–20] including one[13] by the present group. EW relies on electrical modulation of the solid–liquid interfacial tension to control the wettability and motion of water droplets.[21–26]

While several phenomena (droplet growth, droplet coalescence) influence condensation, the key benefit of dropwise condensation is a result of droplet shedding, which exposes fresh areas for re-nucleation, and prevents the formation of a continuous liquid film. The objective of EW-accelerated condensation is to move the condensed liquid into a more favorable state for removal by coalescing droplets to make them large enough for gravity-assisted removal. Under an EW field, coalescence of a distribution of droplets is not continuous.[13,14,18] Rather, coalescence occurs in cascades, wherein droplets coalesce rapidly in a short time interval, followed by a relatively quiet phase (no coalescence), until the droplets grow large enough for the next coalescence cascade.[13] This cycle continues until droplets are larger than the capillary length, at which point they can shed-off under gravity. These observations suggest that a continuous EW field is not necessary, and intermittent EW fields can remove condensate effectively; this premise is studied presently.

This work studies the physics underlying EW-induced shedding of droplets on a hydrophobic surface. More specifically, we study the *details of transient dewetting and quantify dry area fractions and time constants associated with dewetting*. Importantly, we analyze short-duration droplet shedding (right after application of an EW field) in a single coalescence cascade (of droplets); this is in contrast to previous studies, which analyze shedding during continuous condensation. Our experiments lead to several fundamental insights about EW-induced dewetting. While the applied voltage influences the extent of droplet shedding, the rate of droplet shedding is influenced by the frequency of the AC EW waveform. We see that surfaces can be significantly de-wetted (>90% dry) in less than a second. Importantly, the measured water removal rates under EW fields are higher than typical dropwise condensation rates by >100 times. We note that the present study focuses on droplet shedding only and that the results are applicable for condensation and non-condensation environments.

Device fabrication and the experimental procedure are briefly described ahead. Indium Tin Oxide (ITO) coated glass slides were used as the substrate. Photolithography and plasma etching were used to pattern ITO into two sets of interdigitated electrodes [Fig. 1(a)]. These were connected to the high voltage and ground ends of a signal generator and amplifier to generate an electric field in the gap between electrodes [Fig. 1(b)]. A 5 μm layer of SU-8 was spin-coated as the EW dielectric, followed by spin coating of a 100 nm layer of Teflon for hydrophobicity. Fabrication-related details are included in the supplementary material.

The starting ensemble of droplets (to be shed off) was obtained by spraying water on vertically oriented devices using a commercial humidifier. Droplet size distributions obtained were remarkably consistent (average droplet radius was $\sim$150 μm $\pm$ 50 μm). It is striking to observe that the obtained distribution is similar to that obtained in classical dropwise condensation experiments.[27] This justifies the translation of present results to dropwise condensation applications. Post droplet-deposition, the surface was visualized using a stereoscope.

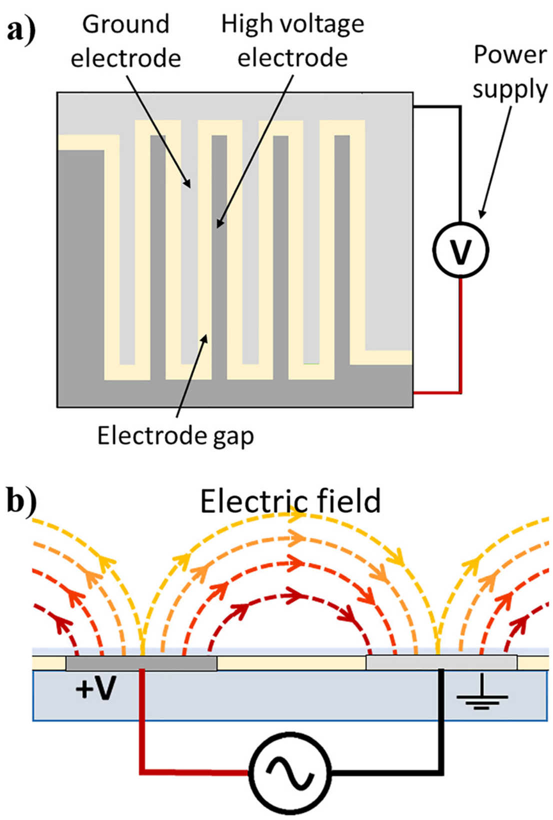

FIG. 1. Schematic showing the arrangement of interdigitated electrodes. (b) Cross-section of the device showing electric field lines.

The EW field was then turned on for 30 s, during which most of the water shed off the surface. Individual droplets were tracked using a MATLAB circle finder code.

Three experimental parameters were varied presently. First, three different electrode geometries were used with electrode widths of 50 μm, 100 μm, and 200 μm; spacing between electrodes was 50 μm in all devices. These two parameters influence the electric field and the penetration height of the electric field outside the surface. The second parameter was the applied voltage, with experiments conducted at 175 V, 200 V, and 300 V. This voltage range was selected to be above the threshold voltage (when droplet shedding is first observed) and the saturation voltage (contact angle stops responding to voltage[21,22]) The third parameter was the frequency of the applied AC waveform. Experiments were conducted at 1 Hz, 10 Hz, and 1 kHz; together this frequency range accounts for various types of fluid motion (ranging from droplet translation to shape oscillation). All experiments were repeated 5 times.

Figure 2 (Multimedia view) (high speed visualizations as multimedia view) shows EW-induced droplet shedding at three frequencies. The extent of droplet shedding is quantified by the dry area fraction, $\Gamma = A_{dry}/A_{total}$. This is estimated via image analysis and represents the fraction of the surface not covered with water. Figure 2 shows that for a 175 V, 1 Hz waveform, Γ increases from 45% to 70%. Importantly, at higher frequencies, almost the entire surface is water-free; 175 V, 1 kHz increases Γ from 43% to 92%. It is noted that a threshold voltage is needed to electrically actuate droplets. In this study, we define the threshold voltage as the voltage, which increases Γ by 20%. For the 50 μm, 100 μm, and 200 μm devices, the threshold voltages were 175 V, 135 V, and 130 V, respectively.

The physics underlying droplet coalescence and shedding is briefly discussed and is related to the reduction in contact angles as per the Young-Lippman equation[21,22] (details in the supplementary material) and the rearrangement of droplets on energy minima positions on the surface.[13,14] The contact angle (CA) vs voltage curve (Fig. S1) shows a larger change in the CA at higher voltages and larger

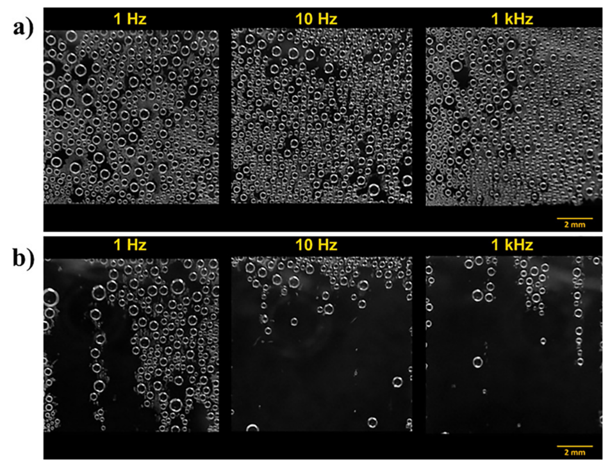

FIG. 2. EW-induced droplet shedding at 175 V, and various frequencies on 100 μm electrode width device. (a) Shows surface before voltage is applied and (b) shows surface 30 s after voltage is applied. Multimedia view: https://doi.org/10.1063/5.0006117.1

electrode widths; this is a consequence of a higher electric field. Presently, EW-induced CA reduction leads to droplet spreading out and coalescing with neighboring droplets. Higher voltages and larger electrode widths lead to greater spreading, which enables more coalescence and faster growth and eventual shedding.

We note that droplet roll-off is also strongly influenced by contact angle hysteresis (CAH), which is the difference between the advancing and receding contact angles.[20] Smaller CAH implies lower frictional forces, which enables gravity-assisted depinning and shedding of droplets at smaller sizes.[8,20,28] On Teflon surfaces (like the present ones), CAH ranges from 9 to 13°[29,30] in the absence of an EW voltage. Li *et al.*[30] showed that EW can lower CAH to up to 3°, with CAH reduction increasing at higher voltages. This highlights the twin benefits of AC EW in our experiments, namely coalescence promotion and reduction in CAH. Both these benefits synergistically enhance droplet shedding.

Under AC electric fields, the nature of droplet motion depends on the AC frequency.[13,31] At low frequencies (frequency < charge relaxation time), droplets mechanically oscillate in response to the sinusoidal field.[31] At frequencies greater than the charge relaxation time, the droplet cannot mechanically respond to the changing field.[31,32] When droplets respond to an EW waveform, they contact neighboring droplets, resulting in a coalescence cascade, which leads to the formation of larger droplets and eventual shedding. Fig. S2 and video S2 (supplementary material) show the influence of three AC frequencies, 1 Hz, 10 Hz, and 1 kHz on a distribution of droplets. At 1 Hz, the droplets move to surface energy minima in response to the sinusoidal wave form, causing coalescence events. At such low frequencies, droplets stay at their stable location for longer, resulting in slower and less frequent coalescence events. At 10 Hz, droplet motion and coalescence events occur ~ 10 times more often per cycle than at 1 Hz frequency, resulting in faster de-wetting. At 1 kHz, all droplets immediately move to the surface energy minima causing an instant coalescence cascade. Additionally, as the AC frequency is higher than the charge relaxation time, the droplet does not translate with the alternating field; instead internal mixing within the droplet occurs.[31,32] The application of an AC field will also oscillate and perturb the three-phase contact line, depinning droplets from the surface, further assisting shedding. Figure S2 clearly shows that 1 kHz has the maximum number of coalescence events followed by 10 Hz and 1 Hz.

Figure 3 shows the influence of voltage and frequency on Γ for the three devices. The bottom of the vertical bar shows the initial Γ ($\Gamma_{t=0s}$) and the top shows the Γ after the experiment ($\Gamma_{t=30s}$). Figure 3 offers several insights into the underlying physical mechanisms. First, very high Γ (> 90%) is obtained at 300 V for all devices; Fig. 3(d) shows that almost the entire surface is water-free, with $\Gamma = 98\%$. In general, Γ increases with voltage, and with larger electrode widths. For electric fields with voltages >200 V and electrode:electrode gap ratios >2, the final Γ was always >85%. Achieving such high values of Γ is challenging without the use of superhydrophobic surfaces.[33] Second, Γ increases rapidly above the threshold voltage. This is most clearly obvious for the 50 μm device, where the Γ is noticeably higher at 200 V, compared to the threshold voltage of 175 V. This is further confirmed from the results of the 100 μm and 200 μm devices, which do not show a large difference in Γ between 200 V and 300 V, noting that the threshold voltages for these devices are 135 and 130 V, respectively. Importantly, these findings show that significant water shedding can be achieved, without needing to use voltages significantly higher than the threshold voltage. Third, the frequency of the AC waveform does not influence Γ at voltages significantly above the threshold voltage; this is observed for all devices. It is noted that the frequency influences Γ only near threshold voltages (Fig. 2), with increasing frequencies resulting in higher Γ's. Overall, these findings show that while the frequency determines the nature of droplet motion, it does not strongly influence Γ, which is primarily determined by the magnitude of the electric field.

In addition to the change in Γ, the rate at which Γ changes is important for applications that require rapid water removal (e.g., windshields). Figure 4(a) shows the transient increase in Γ for the three devices for an applied voltage of 175 V, 10 Hz. The 200 μm device sees a Γ > 90%, whereas the 50 μm device only sees Γ ~70%. This again shows the influence of the electric field (highest for 200 μm device) on droplet shedding.

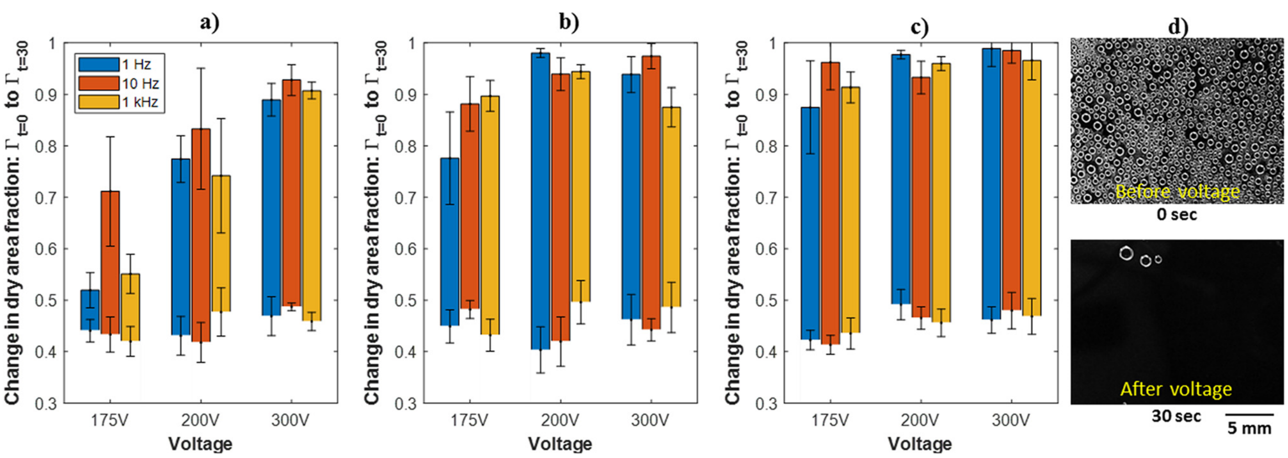

FIG. 3. Change in the dry area fraction due to an EW field on devices with electrode widths of (a) 50 μm, (b) 100 μm, and (c) 200 μm. (d) Highest dry area fraction obtained in this study was 98% at 300 V, 10 Hz on the device with 200 μm electrode width.

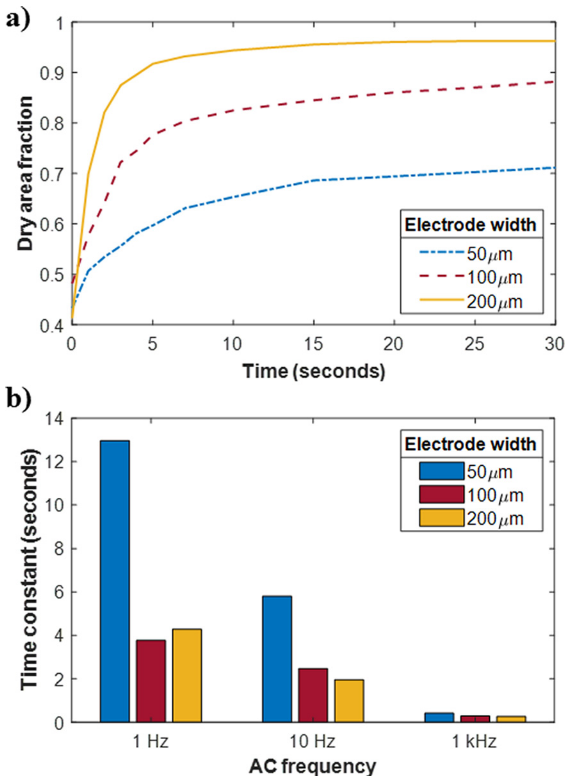

FIG. 4. (a) Transient dry area fraction for three devices at 175 V, 10 Hz, and (b) influence of AC frequency on the de-wetting time constant at 200 V.

Significant physical insights can be obtained by using the data in Fig. 4(a) to define a de-wetting time constant τ; this is a measure of the time taken to reach the steady state Γ. This definition is inspired by comparison with physical systems, which involve transients. τ is estimated by fitting the transient Γ to the below model

$$\frac{\Gamma(t)}{\Gamma_0} = 1 - \exp\left(-\frac{t}{\tau}\right), \tag{1}$$

where Γ_0 is the initial Γ. The steady state is defined as that corresponding to $t = 4\tau$. Physically, τ represents the speed at which the surface is de-wetted and is an important parameter for systems with transient EW fields.

Figure 4(b) shows the frequency-dependent time constant for different devices. At low frequency (1 Hz), the time constant is >4 s. At such frequencies, the droplet mechanically responds to the electric field by shape oscillations and translation. At higher frequencies, (1 kHz) the time constant is <1 s. Such frequencies are higher than the charge relaxation time, and no macroscopic droplet motion is observed after droplets reach the energy minima positions. However, the coalescence cascade[13,14] setup at such frequencies is stronger than the one in the low frequency case, which causes rapid surface cleaning. It is clearly seen via high speed visualization (supplementary material) that 1 kHz has the maximum number of coalescence events, followed by 10 Hz and 1 Hz. It is noted that the time constant is independent of the final Γ. In summary, while Γ is predominantly determined by the voltage, the time required to reach Γ is strongly influenced by the frequency. The supplementary material contains more data on the voltage and frequency dependent τ. At low frequencies, the time constant increases; the τ at a frequency of 1 Hz is 6 times the τ at a frequency of 1 kHz.

It is noted that the electrode orientation plays a notable role in droplet removal. In all the experiments reported so far, the electrodes were vertically oriented (with respect to gravity). For the combination of device and waveform (200 μm electrode width, 300 V at 10 Hz and 1 kHz) that resulted in the highest Γ, additional experiments were conducted with horizontally oriented electrodes. The measured Γ is 4% and 16% less than the vertically oriented electrodes for 10 Hz and 1 kHz, respectively. This can be attributed to electrostatic pinning of droplets on electrodes as droplets move across electrodes (in the horizontal electrode configuration). In contrast, for vertically oriented electrodes, the droplets remain on the same set of electrodes as they slide down, which reduces pinning.

The above findings highlight the rapid removal of water immediately after the application of an EW field; this suggests benefits in using periodic EW fields as opposed to continuous fields. It is insightful to compare the presently obtained mass removal rates with mass removal rates resulting from continuous EW fields and those achieved during classical steady state condensation. Figure 5 provides such a comparison and shows the mass flux vs the electric field. The electric field is estimated as $E \sim \frac{V}{d}$ where V is the voltage and d is the equivalent thickness of the dielectric layer (obtained by fitting the measured change in contact angle to the Lippman's curve). Mass flux in the present study was estimated via image analysis over the duration 4 τ. Figure 5 also includes condensation rate measurements (80% relative humidity) under a continuous electric field using the procedure detailed in a previous study from our group.[13] Additionally, steady state condensation rates from two other studies are also included.[9,33]

The presently obtained mass removal fluxes are 200–400 times higher than condensation rates for continuous electric fields. They are two orders of magnitude higher than those achieved in the absence of an EW field. These numbers suggest that waiting for droplets to grow and then applying an electric field might result in higher overall

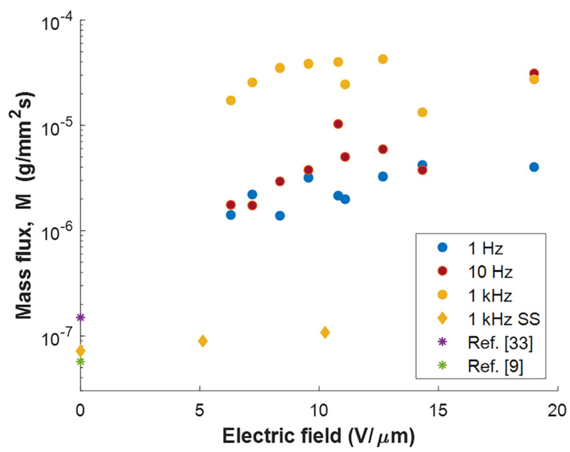

FIG. 5. Mass flux from the present work compared to steady state condensation mass flux under continuous electric fields and no electric fields.[9,33]

condensation rates; however, more detailed studies are needed to validate this hypothesis. Figure 5 also shows that the mass flux increases with the electric field, which is a consequence of a higher Γ. Higher mass fluxes are obtained at 1 kHz as compared to 1 Hz; this can be attributed to the smaller time constants at 1 kHz.

Fundamentally, the mass removal flux can be estimated via a fundamental scaling analysis as $\dot{m}'' \sim \rho r_0 \frac{\Delta a_w}{4\tau}$, where Δa_w is the change in the dry area fraction, ρ is the density, and r_0 is the initial radius. The above formulation shows a reasonable match with the present experimental measurements (details of scaling analysis and results are included in the supplementary material).

In conclusion, this study provides a deeper understanding of the fundamentals underlying EW-induced droplet shedding. It is seen that the voltage and frequency determine the extent and rate, respectively, of water removal. Importantly, dry area fractions approach 100%; this is important considering that the surface is only hydrophobic and not superhydrophobic (which will lead to 100% dryness). The results suggest that the combination of electrowetting and hydrophobic surfaces can give performance enhancements similar to those achieved by superhydrophobic surfaces.

See the supplementary material for (i) details on device fabrication, (ii) details on electrowetting-induced contact angle change in co-planar electrode configuration, (iii) detailed analysis of transients associated with droplet shedding, and (iv) details of the analytical model to predict mass removal flux under electric fields.

The authors acknowledge National Science Foundation Grant No. CBET-1805179 for supporting this work.

DATA AVAILABILITY

The data that support the findings of this study are available from the corresponding author upon reasonable request.

REFERENCES

[1]M. H. M. Grooten and C. W. M. Van Der Geld, "Surface property effects on dropwise condensation heat transfer from flowing air-steam mixtures to promote drainage," Int. J. Therm. Sci. **54**, 220–229 (2012).
[2]V. G. Reifert, A. I. Sardak, S. V. Grigorenko, and V. L. Podbereznyj, "Heat exchange at dropwise condensation in heat exchangers of desalination plants," Desalination **74**, 373–382 (1989).
[3]S. Parekh, M. M. Farid, J. R. Selman, and S. Al-hallaj, "Solar desalination with a humidification-dehumidification technique—A comprehensive technical review," Desalination **160**, 167–186 (2004).
[4]E. D. Wikramanayake, O. Ozkan, and V. Bahadur, "Landfill gas-powered atmospheric water harvesting (AWH) for oilfield operations in the United States," Energy **138**, 647–658 (2017).
[5]K.-C. Park, S. S. Chhatre, S. Srinivasan, R. E. Cohen, and G. H. McKinley, "Optimal design of permeable fiber network structures for fog harvesting," Langmuir **29**, 13269–13277 (2013).
[6]H. Kim, S. Yang, S. R. Rao, S. Narayanan, E. A. Kaupstin, H. Furukawa, S. A. Umans, O. M. Yaghi, and E. N. Wang, "Water harvesting from air with metal-organic frameworks powered by natural sunlight," Science **356**, 430–434 (2017).
[7]J. W. Rose, "Dropwise condensation theory and experiment: A review," Proc. Inst. Mech. Eng., Part A **216**, 115–128 (2002).
[8]N. Miljkovic, R. Enright, and E. N. Wang, "Modeling and optimization of superhydrophobic condensation," J. Heat Transfer **135**, 111004 (2013).
[9]B. Mondal, M. M. G. Eain, Q. Xu, V. M. Egan, J. Punch, and A. M. Lyons, "Design and fabrication of a hybrid superhydrophobic-hydrophilic surface that exhibits stable dropwise condensation," ACS Appl. Mater. Interfaces **7**, 23575–23588 (2015).
[10]Y. Hou, M. Yu, X. Chen, Z. Wang, and S. Yao, "Recurrent filmwise and dropwise condensation on a beetle mimetic surface," ACS Nano **9**, 71–81 (2015).
[11]A. Ghosh, S. Beaini, B. J. Zhang, R. Ganguly, and C. M. Megaridis, "Enhancing dropwise condensation through bioinspired wettability patterning," Langmuir **30**, 13103–13115 (2014).
[12]C. W. Lo, Y. C. Chu, M. H. Yen, and M. C. Lu, "Enhancing condensation heat transfer on three-dimensional hybrid surfaces," Joule **3**, 2806–2823 (2019).
[13]E. D. Wikramanayake and V. Bahadur, "Electrowetting-based enhancement of droplet growth dynamics and heat transfer during humid air condensation," Int. J. Heat Mass Transfer **140**, 260–268 (2019).
[14]D. Baratian, R. Dey, H. Hoek, D. Van Den Ende, and F. Mugele, "Breath figures under electrowetting: electrically controlled evolution of drop condensation patterns," Phys. Rev. Lett. **120**, 214502 (2018).
[15]R. Dey, J. Gilbers, D. Baratian, H. Hoek, D. van den Ende, and F. Mugele, "Controlling shedding characteristics of condensate drops using electrowetting," Appl. Phys. Lett. **113**, 243703 (2018).
[16]R. Yan and C.-L. Chen, "Condensation droplet distribution regulated by electrowetting," J. Heat Transfer **141**, 111501 (2019).
[17]R. Yan, T. S. McClure, I. H. Jasim, A. K. R. Koppula, S. Wang, M. Almasri, and C.-L. Chen, "Enhanced water capture induced with electrowetting-on-dielectric (EWOD) approach," Appl. Phys. Lett. **113**, 204101 (2018).
[18]S. Högnadóttir, K. Kristinsson, H. G. Thormar, and K. Leosson, "Increased droplet coalescence using electrowetting on dielectric (EWOD)," Appl. Phys. Lett. **116**, 073702 (2020).
[19]J. Kim and M. Kaviany, "Electrowetting purged surface condensate in evaporators," Heat Transfer Eng. **31**, 101–107 (2010).
[20]J. Kim and M. Kaviany, "Purging of dropwise condensate by electrowetting," J. Appl. Phys. **101**, 103520 (2007).
[21]F. Mugele and J.-C. Baret, "Electrowetting: From basics to applications," J. Phys.: Condens. Matter **17**, R705–R774 (2005).
[22]L. Chen and E. Bonaccurso, "Electrowetting—From statics to dynamics," Adv. Colloid Interface Sci. **210**, 2–12 (2014).
[23]G. Lippmann, *Relations Entre les Phénomènes Électriques et Capillaires* (Gauthier-Villars, 1975).
[24]V. Bahadur and S. V. Garimella, "An energy-based model for electrowetting-induced droplet actuation," J. Micromech. Microeng. **16**, 1494–1503 (2006).
[25]N. Kumari, V. Bahadur, and S. V. Garimella, "Electrical actuation of electrically conducting and insulating droplets using ac and dc voltages," J. Micromech. Microeng. **18**, 105015 (2008).
[26]D. t Mannetje, F. G. Mugele, and H. T. M. Van Den Ende, "Stick-slip to sliding transition of dynamic contact lines under ac electrowetting," Langmuir **29**, 15116–15121 (2013).
[27]J. W. Rose, "Dropwise condensation theory," Int. J. Heat Mass Transfer **24**, 191–194 (1981).
[28]H. Cha, H. Vahabi, A. Wu, S. Chavan, M. K. Kim, S. Sett, S. A. Bosch, W. Wang, A. K. Kota, and N. Miljkovic, "Dropwise condensation on hydrophilic surfaces," Sci. Adv. **6**, eaax0746 (2020).
[29]J. Hong, S. J. Lee, B. C. Koo, Y. K. Suh, and K. H. Kang, "Size-selective sliding of sessile drops on a slightly inclined plane using low-frequency AC electrowetting," Langmuir **28**, 6307–6312 (2012).
[30]F. Li and F. Mugele, "How to make sticky surfaces slippery: Contact angle hysteresis in electrowetting with alternating voltage," Appl. Phys. Lett. **92**, 244108 (2008).
[31]F. J. Hong, D. D. Jiang, and P. Cheng, "Frequency-dependent resonance and asymmetric droplet oscillation under ac electrowetting on coplanar electrodes," J. Micromech. Microeng. **22**, 085024 (2012).
[32]R. Malk, Y. Fouillet, and L. Davoust, "Rotating flow within a droplet actuated with AC EWOD," Sens. Actuators, B **154**, 191–198 (2011).
[33]I. Nayshevsky, Q. Xu, and A. M. Lyons, "Hydrophobic-hydrophilic surfaces exhibiting dropwise condensation for anti-soiling applications," IEEE J. Photovoltaics **9**, 302–307 (2019).